Biogeochemistry (2024) 167:1533–1552
https://doi.org/10.1007/s10533-024-01184-6

Iron as a precursor of aggregation and vector of organic carbon to sediments in a boreal lake

Simon David Herzog · Viktoriia Mekelesh · Margarida Soares · Ulf Olsson · Per Persson · Emma Sofia Kritzberg

Received: 29 April 2024 / Accepted: 29 September 2024 / Published online: 15 October 2024

Abstract While organic matter (OM) interactions in the water column prevent iron (Fe) precipitation and sedimentation, Fe also acts as a precursor of aggregation and a vector of OM to sediments. This study aims to characterize Fe–OM interactions to understand the role of Fe in promoting aggregation and transport of OM. Samples of Fe and OM were collected from water, settling material, and sediment along a gradient starting from the inlet and continuing offshore within a boreal lake. Fe speciation was determined using X-ray absorption spectroscopy (XAS), and the chemical composition of OM was assessed using Diffuse reflectance infrared Fourier transform spectroscopy (DRIFT IR) and Nuclear magnetic resonance spectroscopy (NMR). The results show a decrease in Fe and OM concentrations in the water column with increasing distance from the inlet. Winter sampling revealed a shift in Fe speciation from dominance of organically complexed Fe to an increase in Fe(oxy)hydroxide, accompanied by a loss of aromatic and carboxylate function of OM. Summer sampling revealed no significant changes along the gradient, with Fe(oxy)hydroxide and carbohydrates dominating the water phase. Interestingly, settling particles and surface sediments were dominated by Fe(oxy) hydroxides and aliphatic OM. We propose that phototransformation may be an important process that influences the interaction between Fe and OM and, as a consequence, their fate along the spatial gradient. Our study suggests a photochemically induced loss of carboxylate groups, reflected by an increased carbohydrate-to-carboxylate ratio along the gradient, particularly in winter, and generally lower levels during summer. Loss of carboxylate function promotes the

Responsible Editor: Susan Ziegler.

Supplementary Information The online version contains supplementary material available at https://doi.org/10.1007/s10533-024-01184-6.

S. D. Herzog (✉)
Department of Science and Environment, Environmental Dynamics, Roskilde University, 4000 Roskilde, Denmark
e-mail: sherzog@ruc.dk

S. D. Herzog · M. Soares · E. S. Kritzberg
Department of Biology/Aquatic Ecology, Lund University, 223 62 Lund, Sweden
e-mail: margarida.soares@biol.lu.se

E. S. Kritzberg
e-mail: emma.kritzberg@biol.lu.se

V. Mekelesh · P. Persson
Centre for Environmental and Climate Research & Department of Biology, Lund University, 223 62 Lund, Sweden
e-mail: viktoriia.meklesh@cec.lu.se

P. Persson
e-mail: per.persson@cec.lu.se

U. Olsson
Department of Chemistry, Physical Chemistry Division, Lund University, 22362 Lund, Sweden
e-mail: ulf.olsson@fkem1.lu.se

formation of Fe(oxy)hydroxides, which in turn, facilitates the aggregation and sinking of OM, particularly aliphatic components. These insights contribute to a broader understanding of carbon cycling and storage in lakes. Future studies should assess the significance of photochemical processes to OM burial and it how may change given trends in Fe and OM in northern regions.

Keywords Iron (Fe) speciation · Organic matter (OM) composition · Fe–OM interactions · Boreal lake · Photochemical processes · Carbon cycling

Introduction

Browning of freshwaters is a widely reported phenomenon in northern regions, and is attributed to rising concentrations of dissolved organic matter (OM) and iron (Fe) originating from the catchment (Monteith et al. 2007; Kritzberg and Ekstrom 2012; Sarkkola et al. 2013; Weyhenmeyer et al. 2014; Björnerås et al. 2017; Xiao and Riise 2021). One of several effects of browning is that it can alter the biogeochemical fate of terrestrially derived organic carbon, which accounts for about half of dissolved OM, e.g. whether it is remineralized and emitted to the atmosphere, stored in sediments or transported downstream (Tranvik et al. 2009). The loading of OM has direct consequences in this respect, e.g. CO_2 emissions are higher from waters with higher OM concentration (Larsen et al. 2011). In addition, Fe has the capacity to influence key processes that are decisive to the fate of organic carbon (OC) in aquatic systems. These processes include photochemical transformations (Gu et al. 2017), aggregation of dissolved organic carbon into particles (von Wachenfeldt and Tranvik 2008; Porcal et al. 2013), and preservation of organic carbon in sediments (Lalonde et al. 2012; Barber et al. 2017). However, the quantitative importance and the mechanisms by which Fe influences OM transformation and loss processes, especially in freshwaters, remain poorly understood.

Fe and OM are tightly coupled in boreal surface waters (Köhler et al. 2013; Weyhenmeyer et al. 2014; Blazevic et al. 2016). Interactions with OM promote the stability of Fe in freshwaters (Shapiro 1966; Vindedahl et al. 2016), either by the formation of mononuclear organic Fe complexes (Fe-OM), or by surface interactions with Fe(oxy)hydroxides (Hassellöv et al. 1999; Lyvén et al. 2003; Sundman et al. 2013; Vindedahl et al. 2016). These two phases dominate total aqueous Fe in boreal waters (Herzog et al. 2017; Karlsson et al. 2008). At the same time, aggregation of Fe-associated OM is proposed to act as a precursor of sediment formation in boreal lakes (von Wachenfeldt and Tranvik 2008). In fact, lakes are efficient Fe sinks. In large boreal lakes, most of the incoming Fe is reported to be lost to sediments (e.g. 77% in Lake Bolmen (Björnerås et al. 2021) and 95% in Lake Mälaren (Köhler et al. 2013)). Not much is known about what controls the fate of Fe in lakes, or how it connects with the fate of OM. In a study of Lake Bolmen in southern Sweden, inflowing stream waters contained Fe–OM, but in sediments only minerogenic Fe phases, like Fe(oxy)hydroxide, Fe-bearing silicate and clay fractions, were found (Björnerås et al. 2021). Other studies have also found high contributions of Fe(oxy)hydroxide in lake sediments (Spadini et al. 2003; Sun et al. 2018), suggesting that lake sediments are a sink for mainly minerogenic Fe. Along with Fe loss to sediments, also OM removal is observed, though to a lesser extent (Björnerås et al. 2021; Köhler et al. 2013). Translocation of OM to sediments is proposed to be linked to formation of aggregates through metal interactions (Kellerman et al. 2015; Guillemette et al. 2017). Aromatic compounds with carboxylate functionality have particularly high affinity for Fe(oxy)hydroxide (Kleber et al. 2015; Coward et al. 2018), and co-transport with Fe has been suggested to at least partially explain the preferential loss of aromatic OM along the aquatic continuum (Köhler et al. 2013; Kothawala et al. 2014).

The longer residence time in lakes compared to streams provides a critical opportunity for physical, chemical and biological processes to occur. This can enhance the removal of both dissolved OM and Fe, particularly in boreal lakes where concentrations tend to be higher (Weyhenmeyer et al. 2014; Xiao and Riise 2021). Transformation processes induced by solar radiation (Drozdova et al. 2020; Gu et al. 2017) and changes in pH (Karlsson and Persson 2012), have been proposed to change the interaction between Fe and OM and promote flocculation and sedimentation (von Wachenfeldt and Tranvik 2008; Helms et al. 2013). Research on transformation processes of Fe and OM has predominantly been

restricted to laboratory studies, which focus either on the OM characterisation or the Fe speciation without connecting them (Karlsson and Persson 2012; Helms et al. 2013; Drozdova et al. 2020). Development of advanced analytical tools and the integration of their use in environmental science have moved us to a point where understanding of Fe–OM interactions can be greatly progressed.

The aim of the current study was to describe the nature of interactions between Fe and OM, and to capture how transformations of Fe and OM influence their biogeochemical fate in a natural system. A particular focus was on the role of Fe as a precursor of aggregation and a vector of OM to sediments. Lake Bolmen was chosen as a study system, and previous studies have shown that Fe concentrations have doubled in this lake over the past 60 years, and that 77% of the Fe in inflowing water is lost to the sediment during transit through the lake (Björnerås et al. 2021). To probe the interactions between Fe and OM, we sampled along a gradient of increasing distance from the main inlets of Lake Bolmen (Fig. 1). We collected water from surface and bottom, sinking material in sediment traps, and accumulated material from sediment cores. Sampling was conducted once in winter during high-flow and once in summer during low-flow. The samples were analyzed to establish concentrations and fluxes of Fe and OM, the speciation of Fe by X-ray absorption spectroscopy (XAS), the composition of the OM by Diffuse reflectance infrared Fourier transform (DRIFT) spectroscopy and complementing with carbon and hydrogen NMR.

We hypothesized that in lake processes would decrease the contribution of Fe–OM and consequently increase the Fe(oxy)hydroxide fraction in the water column with increasing distance from the inlet, and that Fe(oxy)hydroxides would be preferentially lost by sinking. This would result in declining Fe concentrations in the water column with increasing distance from the inlet, and dominance of Fe(oxy) hydroxides in sediment traps and surface sediment. We also expected sinking Fe(oxy)hydroxides to be associated with predominantly aromatic organic compounds with a high density of carboxyl groups. This would result in a preferential removal and dominance of aromatic compounds in sediment traps and sediments.

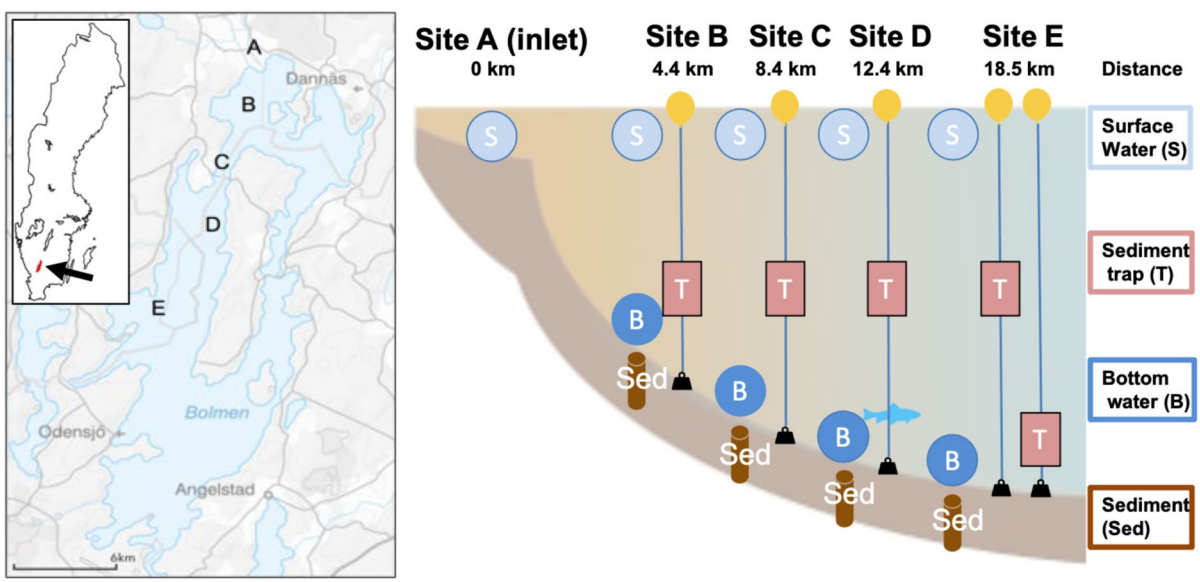

Fig. 1 The location of lake Bolmen in Sweden (arrow) and the sampling sites (left) A: N57.079186° E13.736622°; B: N57.045950° E13.732630°; C: N57.01283° E13.70823°; D: N56.97739° E13.70231° and E: N56.92928° E13.65203° and the sampling scheme (right)

Material and methods

Site description and sampling design

Lake Bolmen is a mesotrophic lake in Småland in southern Sweden (56°55′N 13°40′E). The lake has an area of 184 km^2 and an average and maximum depth of 5.4 and 37 m respectively. The theoretical water residence time of the lake is approximately 1.6 years (Lindström et al. 2018). The large fetch of the lake, in combination with mild winter climate in the region, means the lake rarely freezes. The catchment area is 1640 km^2 and land-cover is dominated by coniferous forest, including large areas of peat particularly in the northern part of the catchment, and minor areas with agricultural and industrial activities. Several small streams drain into Lake Bolmen, but the main inlet is River Storån in the north, which contribute with approximately 70% of the total inflow of Fe and total organic carbon (TOC) (Björnerås et al. 2021). The second largest tributary is River Lillån just west of Storån. We sampled five locations, where site A is the main inlet Storån, and sites B, C, D and E are located at increasing distance of up to 18.5 km from the inlet (Fig. 1). Maximum depth varied from 14 m at site B to 22 m at site E. Sampling took place during two surveys on the 10th of December 2019 (winter) and on 13th of August 2020 (summer). The period preceding the winter sampling was wet (precipitation and evapotranspiration within the catchment 93 and 26 mm during November), with a high discharge of 20.1 m^3/s from the main inlet, while the period preceding summer sampling was dry (65 and 71 mm in August) with a discharge of 4.1 m^3/s at the inlet (https://vattenwebb.smhi.se/).

Water column sampling

Depth profiles of temperature, and dissolved oxygen (DO) were obtained using a CTD probe (AAQ1186s-H, Alec Electronics). Surface water samples were collected 0.5 m below the surface and immediately stored in acid-washed polyethylene containers. Bottom water samples were collected with a Ruttner sampler approximately 1.5 m above the lake sediment (Fig. 1). Samples were filtered through a 50-µm mesh, and stored cold and dark in a cooling box for no more than 5 h until return to the lab for further analysis. A 1-l subsample from all locations was freeze-dried and later used for XAS analyses. All equipment for sample handling was acid cleaned (24 h in 10% HCl (TraceMetal™ Grade Fisher Chemical™) and rinsed with Milli-Q water). In the lab pH was measured on a 913 pH Meter (Metrohm).

Sediment traps

In summer, sediment traps were installed at sites B, C, D and E and left for 12 days at a depth of 7 m. At site E, which was the only site with a temperature gradient, an additional sediment trap was installed at 1.5 m above the sediment (Fig. 1). Each sediment trap consisted of eight 39-cm long polycarbonate tubes with an inner surface area of 15.2 cm^2, sealed with a rubber stopper at the bottom. The sediment trap was attached to a rope anchored in the sediment and to a buoy placed 1 m under the water surface, to keep the trap fixed in a vertical position. At collection of the traps the opening of the tubes were sealed with a rubber stopper. The sealed tubes were kept dark and cold during transport to the lab. The tubes recovered from the bottom sediment trap located at site E were immediately frozen upon sampling in a dry ice-ethanol bath and stored frozen until further analysis. In the laboratory, the particulate material within the tubes was allowed to settle for 24 h whereupon the bulk of the supernatant water was removed using a peristaltic pump. The remaining water and particles were transferred into 50-ml Falcon tubes and separated from the remaining supernatant by centrifugation (4200 *g* for 15 min at 4 °C). The particulate material was freeze-dried, weighed and stored under dry and dark conditions until further analysis. Sinking rates were calculated by dividing the sediment weight (mg) by the trap tube sedimentation area (cm^2) and the deployment time (y).

Sediment sampling

Two sediment cores per site were collected at sites B, C, D and E using an HTH gravity corer for soft sediments (Renberg and Hansson 2008), both during the winter and the summer survey. One core was immediately frozen, stored, and later used for C-NMR and XAS analysis. The second core

was sliced into 1-cm sections, with each section being kept cold and in an individual container during transport to the lab where the samples were weighed and freeze-dried. The freeze-dried samples were used for elemental analysis of the sediments.

Elemental analysis

Total Fe concentrations were determined in water and particles from sediment traps and sediments with ICP-OES (Perkin Elmer Optima 8300). Liquid samples were acidified (1% HNO_3; TraceMetal™ Grade Fisher Chemical™) 24 h prior to analysis. Solid samples were freeze dried and digested in 7 M HNO3, which extracts all Fe except such incorporated in the silicate crystalline lattice and measured according to SS-28311 (2017). Total C and N content in solid samples were measured using a Costech ESC 4010 elemental analyser. Concentration of organic carbon as total organic carbon (TOC) in the water samples was analysed using the non-purgeable organic matter method (Shimadzu TOC V-CPN). Samples were acidified to $pH < 2$ with 2 M HCl.

Optical properties

Spectral absorbance (200–900 nm) was measured using a Beckman Coulter DU-800 spectrophotometer using a 1 cm quartz cuvette and MilliQ water as a baseline reference. We used Abs at 420 nm as proxy for water colour, specific ultraviolet absorbance at 254 nm (SUVA) as an indicator of aromaticity (Weishaar et al. 2003), and the ratio of the absorbance measured at 250 and 365 nm (E2:E3) as well as the spectral slope ratio (S_R; Helms et al. 2008), were used as a proxy of the average molecular weight of coloured dissolved organic matter (CDOM) and the latter also for photochemically induced shifts in MW (De Haan and De Boer 1987; Helms et al. 2008). For S_R, the ratio of the slope coefficient (S) calculated for UVB (275–295 nm) and UVA (350–400 nm) wavelengths ($S_R = S_{275–295}/S_{350–400}$), was modeled in R (Team 2013) using the package CDOM (version 0.1; (Massicotte and Markager 2016)). Additionally, the ratio between the wavelengths 254 and 436 nm (E2:E4) was used to provide an estimation about the relative composition of autochthonous vs. terrestrial DOM (Battin 1998) and the intensity of UV-absorbing functional groups compared to the coloured ones (Uyguner and Bekbolet 2005). Chlorophyl-a (Chl-a) concentration was measured immediately upon arrival in the lab on a fluorometer (AlgaeLabAnalyser fluorometer, bbe moldaenke).

XAS sample treatment, data collection and analysis

For the determination of the Fe speciation in water, settling particles and sediment samples were frozen, then freeze dried and homogenised using a mortar and pestle before either mounting in a sample holder or pressing into a pellet. A subset of samples from the settling particle (site E) and sediments samples (site B and E) were stored intact and frozen and measured in this state of matter.

XAS spectra on the Fe K-edge of winter samples were collected at the beam line 4–1 at the Stanford Synchrotron Radiation Lightsource (SSRL) in Stanford, US. The XAS spectra of summer samples were collected at the beam line Balder at MaxIV at MaxLab Lund, Sweden. Between two to four scans were collected, depending on the Fe concentration, at the Fe K-edge up to the k range of 14 $Å^{-1}$ in either fluorescence or transmission mode. At SSRL a transmission spectra of a reference Fe foil simultaneously during all was recorded, whereas at Balder Fe reference foil spectra were recorded before and after each shift, to allow energy calibration. Viper was used for energy calibration and averaging of the scans data and XANES dactyloscope (Klementiev 2000) to qualitatively compare the X-ray absorption near edge structure (XANES) regions. For the estimation of the proportions of various Fe phases a linear combination fitting (LCF) analysis was applied using the software Sixpack (Webb 2005). For the LCF analysis on XANES and k3-weighted EXAFS spectrum in the k range from 3.0 to 12.0 A^{-1}, model compound spectra from Fe(oxy)hydroxides (ferrihydrite, lepidocrocite, goethite and hematite), organically complexed Fe (Fe(III) complexed to Suwannee Rives fulvic acid) and phyllo- and inosilicates (hornblende, nontronite, vermiculite and ferrosmectite) were selected as references, based on previous studies in boreal freshwater system (Herzog et al. 2019; Sundman et al. 2014; Björneråas et al. 2021). For the LCF analysis, E_0 was allowed to float, and a non-negative boundary condition was used. During

fitting, the sum was not forced to equal 1, but was adjusted afterwards. All components with a contribution of < 5% were excluded from the results. Data treatment including energy calibration and normalization as well as the use of the same reference spectra allows for direct comparison between spectra collected at SSRL and MaxIV. For more details on the XAS analysis see Supporting information section S4 XAS methods.

Infrared spectroscopy (IR)

Water, sediment trap and sediment samples were measured using diffuse reflectance Fourier-transform infrared (DRIFT IR) spectroscopy. The spectra were recorded with Bruker IR spectrometer (VERTEX 70/70v; Bruker, Billerica, Massachusetts) equipped with Praying Mantis™ Diffuse Reflection accessory. The measurements were performed under vacuum and at room temperature. The freeze-dried sample was mixed with KBr (Merck, Uvasol CAS no. 7758-02-3, Darmstadt, Germany) in the proportion of 98–2 mg of KBr/DOM and thoroughly grounded before placing into the sample cup. The DRIFT IR spectra were recorded in the region from 4000 to 400 cm^{-1} with 128 scans per sample and a resolution of 4 cm^{-1}. The baseline spectral correction was done using the spline interpolation method in the Origin software (v. Pro 2018).

^{1}H NMR spectroscopy

High-resolution ^{1}H spectra were collected on a Bruker Avance III HD 500.17 MHz spectrometer (Bruker, Germany) equipped with a 5-mm broadband probe. Water samples were freeze-dried and redissolved in Milli-Q water to obtain a total concentration of 2 g/L. The redispersed freeze-dried water samples dissolved readily and showed no traces of excess insoluble material as seen by visual inspection. To suppress a strong water peak, samples were mixed with deuterium oxide D_2O (99.8%, Armar Chemicals, Switzerland) and a water-suppression pulse sequence was applied (Hwang and Shaka 1995). Samples had a final volume of 0.5 ml and composition of 90–10% in v/v of preconcentrated water samples/D_2O. All experiments were performed at 25 °C with 1024 scans per spectrum. The FID signal was baseline corrected (zero-order and first-order) and processed with 2 Hz of apodization before Fourier transformation. The ^{1}H chemical shifts were calibrated using the residual HDO peak at 4.694 ppm. The relative intensity distribution was obtained from integration of the six spectral regions (Whitty et al. 2021; Wilson 1981): (1) aliphatic, R-CH_3, R-CH_2–R (0.6–1.65 ppm); (2) aliphatic, CH_3COO^- and CH_3COO-R (1.65–2.2 ppm); (3) aliphatic (carboxyl-rich alicyclic molecules, CRAM, Hertkorn et al. 2006), HC-C = Y, *a* protons to carboxyl, carbonyl groups, and aromatic ring, HC-X, protons next to nitrogen or halogen atom (2.2–3.0 ppm); (4) carbohydrate, HC–O–R, *a* protons to carbon attached to oxygen groups, carbohydrates, alcohols, ether (3.0–4.3 ppm); (5) aromatic, Ar–H, aromatic protons including quinones, phenols and ammonium protons (6.0–7.8 ppm), N–H; (6) aromatic, $HCOO^-$ (format), sterically hindered protons of aromatics, nitrogen heteroaromatics (7.8–9.0 ppm).

δ^{13}C natural abundance

Water samples, settling material collected in sediment traps and sediment core samples were analysed for ^{13}C natural abundance, providing information on C sources of allochthonous versus autochthonous origin. Freeze dried samples were ground, weighed and encapsulated whole into tin (Sn) capsules and sent for analysis to University of California, Davis, USA. Solid δ^{13}C samples were analysed on a Hydra Elementar vario MICRO cube elemental analyser (Elementar Analysensysteme GmbH, Langenselbold, Germany) interfaced to a Sercon Europa 20–20 isotope ratio mass spectrometer (Sercon Ltd., Cheshire, United Kingdom) at University of Cailfornia, Davis, USA. For more details see Supporting information section S3 δ^{13}C *Natural Abundance analysis*.

Sediment dating

Freeze dried samples of the sediment cores were used for ^{210}Pb chronological dating by direct radionuclide gamma assay at the Environmental Radiometric Facility at University College London (Appleby 1978). The chronological dating was achieved with a Constant Rate of Supply Model (Appleby 2002) and allowed for the estimation of sedimentations rates. By combining sedimentation rates and the elemental concentrations we estimated elemental accumulation rates in sediment cores.

Statistical analysis

Comparison between surface and bottom water samples, as well as between winter and summer, were made by paired *t*-tests for pH, total Fe, total organic carbon, Oxygen, Absorbance, Temperature, SUVA, S_R, E2:E3, and E2:E4 ratio. Water chemistry data were further explored with Principal Component Analysis (PCA) to obtain a reduced number of variables (multivariate axes) from all samples, which allowed us to better understand how in-lake processes impact the water chemistry. The normality of $\delta^{13}C$ data was assessed and confirmed, and the averaged data are presented with standard deviation. Differences in $\delta^{13}C$ between water, sediment traps, and surface sediments, as well as between winter and summer water samples, were tested using an unpaired *t*-test. This analysis helps determine variations in $\delta^{13}C$, which can provide insights into the sources and seasonal variations of the OM. A one-way analysis of variance (ANOVA) was used to test differences between sedimentation rates in sediment traps, followed by a Tukey HSD test, providing information on the removal processes between the lake sites. The statistical goodness-off-fit parameters for the LCF analysis was used for the XAS analysis to determine the Fe speciation and are reported as chi-square (χ^2).

Results

Temporal and spatial variation in water chemistry

At the time of winter sampling the water was around 4 °C, and the water column was fully oxygenated (Table 1). A well mixed water column was supported by a PCA analysis of the water chemistry variables where the bottom and surface samples for each site were adjacent (Fig. 2a). At the time of summer

Table 1 Hydro-chemical variables in surface and bottom water of winter and summer samples)

	Site	Winter					Summer				
		A	B	C	D	E	A	B	C	D	E
Total Fe (mg/L)	Surface	1.95	1.16	1.04	0.59	0.39	0.59	0.33	0.35	0.20	0.22
	Bottom		1.10	1.00	0.60	0.40		0.68	0.38	0.28	0.62
TOC (mg/L)	Surface	24.7	17.7	16.8	14.8	12.7	12.5	10.6	10.5	10.3	10.9
	Bottom		18.1	17.3	14	11.5		10.6	10.4	10.3	11.4
Abs coeff (420 nm/cm)	Surface	0.173	0.113	0.093	0.057	0.039	0.087	0.052	0.055	0.042	0.036
	Bottom		0.109	0.096	0.059	0.042		0.061	0.042	0.043	0.056
SUVA (L/mg/m)	Surface	6	5.4	5.0	3.8	3.3	5.9	4.3	4.5	4.3	4.0
	Bottom		5.3	4.9	4.1	3.7		4.9	4.6	4.5	4.9
E2:E3 ratio	Surface	3.9	3.9	4.0	4.3	4.6	3.8	3.8	3.8	4.1	5.0
	Bottom		4.0	4.0	4.3	4.6		4.2	4.8	4.8	4.4
E2:E4 ratio	Surface	10.6	10.4	11.1	12.1	13.3	10.4	10.5	10.0	13.0	15.4
	Bottom		10.9	10.9	12.0	12.6		10.3	13.9	13.3	12.4
S_R	Surface	0.69	0.71	0.70	0.74	0.77	0.76	0.99	1.00	0.94	0.88
	Bottom		0.70	0.71	0.73	0.78		0.97	0.89	0.90	0.82
pH	Surface	5.8	6.8	6.9	7.0	7.1	7.1	7.2	7.2	7.2	7.3
	Bottom		6.8	6.8	7.0	7.1		7.1	6.9	6.8	6.9
Oxygen (mg/L)	Surface	10.8	12.6	10.6	12.2	10.6	6.8	8.3	7.9	8.3	9.4
	Bottom		12.2	11.1	12.3	11.3		7.9	5.5	5.6	0.3
Temperature (°C)	Surface	3.7	3.7	3.8	4.7	4.4	17.1	18.7	19.2	19.5	21.9
	Bottom		3.7	3.9	4.1	4.4		17.8	17.5	17.3	13.6
Fe:OC molar-ratio	Surface	0.017	0.014	0.013	0.009	0.007	0.010	0.007	0.007	0.004	0.004
	Bottom		0.013	0.012	0.009	0.008		0.014	0.008	0.006	0.012
Chl a (µg/L)	Surface	0.1	0.8	0.9	1.2	1.3	4.9	7.0	7.2	9.3	n.a

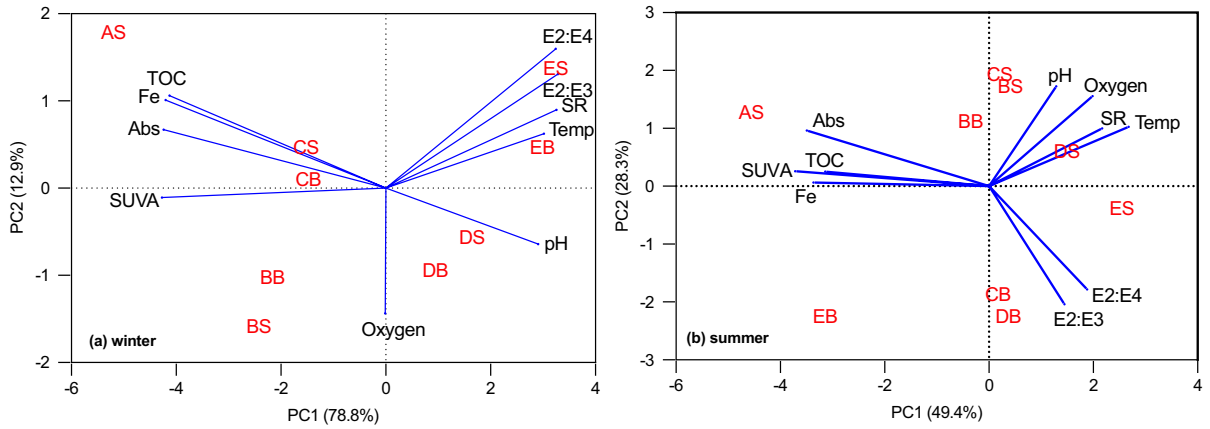

Fig. 2 PCA biplots of winter (left panel) and summer (right panel), where correlations between variables and between variables and the principal components (PC, blue) were combined with the positioning of the data from the sampled sites A–E (red)

sampling, the water temperature varied from 14 to 22 °C, and surface and bottom samples were separated based on differences in temperature, oxygen, pH, E2:E3 E2:E4 and S_R (Fig. 2b). Hypoxic conditions were detected only in the bottom water of the deepest site (EB).

The loss of both Fe and OM from the water column was gradual throughout the entire gradient (A to E) during the high-flow conditions in winter. Concentrations of Fe during low flow conditions in summer were lower, the gradual loss was less pronounced, and there was a tendency to bottom water enrichment. TOC concentrations during summer were also lower, with the highest values measured in the inlet, and little variation was observed among the lake sites (Table 1 and Fig. 3). The loss of Fe along the spatial gradient was larger than that of OC, reflected as a decrease in the Fe:OC molar-ratios during both seasons (Table 1), with exception of the bottom summer samples at site E, which showed an increase in Fe concentration. Further, Abs420 was higher and S_R lower during winter sampling than in summer (Table 1). Similar to Fe and TOC concentration, the inlet was distinct from the lake sites with higher Abs420 and SUVA, and lower pH and S_R, in both the winter and summer survey. In winter, E2:E3, E2:E4 and S_R increase with increasing distance from the inlet and in line with the PCA (Fig. 2).

Sinking and accumulation rates

Fe and C represented the largest elemental fractions in the particles captured by the sediment traps as well as in the sediments, followed by Al and Mn (Table S1 and S2). The sinking rate of Fe in sediment traps was 6–8 and 2–10 times higher than Al and Mn respectively. Fe accumulation rate in surface sediments was 6–17 times and 8–84 times higher than Al and Mn, respectively. Sinking rates of Fe and C were at least two-fold higher near the inlet (sites B and C) compared to downstream (sites D and E; one-way ANOVA: $p < 0.0001$), and sediment accumulation rates of Fe were slightly higher at sites B and C (Fig. 4). When comparing Fe and C rates, Fe:C molar-ratios in the sediment traps were slightly higher at site B and C (0.16 and 0.18) than at site D and E (0.12 and 0.14) (see Table S1). A similar trend was observed in the sediments, where the Fe:C molar-ratios were three-fold higher close to the inlet at site B (1.32) compared to sites C, D and E (lower than 0.38).

Phytoplankton biomass, $\delta^{13}C$ natural abundance and E2:E4 ratio

Chl-a was ~ 1 µg L^{-1} in winter and ~ 7 µg L^{-1} in summer and slightly increasing with increasing distance from the main inlet in summer (Table 1). The $\delta^{13}C$ in the aqueous OM was on average − 27.4 ± 0.6 and somewhat lower in sediment traps samples (− 28.8 ± 0.2; $t_{20} = 4.75$; $p = 0.001$) and

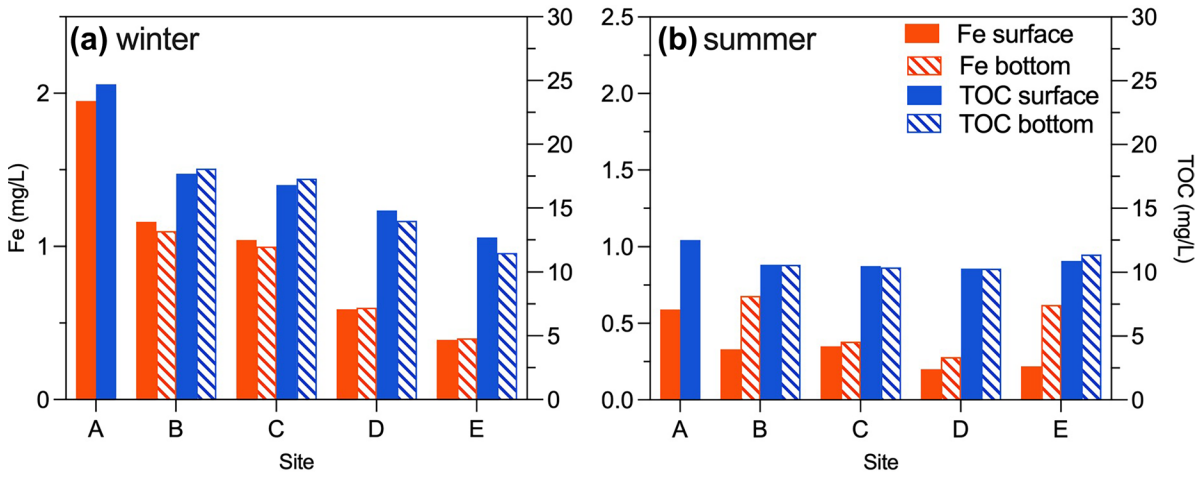

Fig. 3 Fe and TOC concentration in surface and bottom water samples at the sampling sites of winter (**a**) and summer (**b**)

surface sediments (-28.8 ± 0.3; $t_{24} = 6.26$; $p < 0.001$) (Table S3). There was also a small difference in the aqueous OM with lower values observed in the summer (-27.8 ± 0.6) compared to winter (-27.0 ± 0.2) (Table S3; $t_{16} = 3.76$; $p = 0.0017$). Overall all samples were close to the terrestrial $\delta^{13}C$ in boreal ecoregions, which is around -27 (Lajtha and Michener 1994). E2:E4 ratios were overall low, in line with dominance by terrestrial derived DOM (Ilina et al. 2014). Furthermore, E2:E4 ratios increased from A to E during both seasons, and peaked during summer in the surface water at site E (Table 1).

Iron speciation

LCF of the EXAFS data were used to identify the Fe speciation in the water column, sinking material and surface sediments. Fe–OM was strongly dominating in the inlet water (site A) at the time of winter sampling, but with increasing distance from the inlet (site B–E) the contribution of Fe–OM in the water

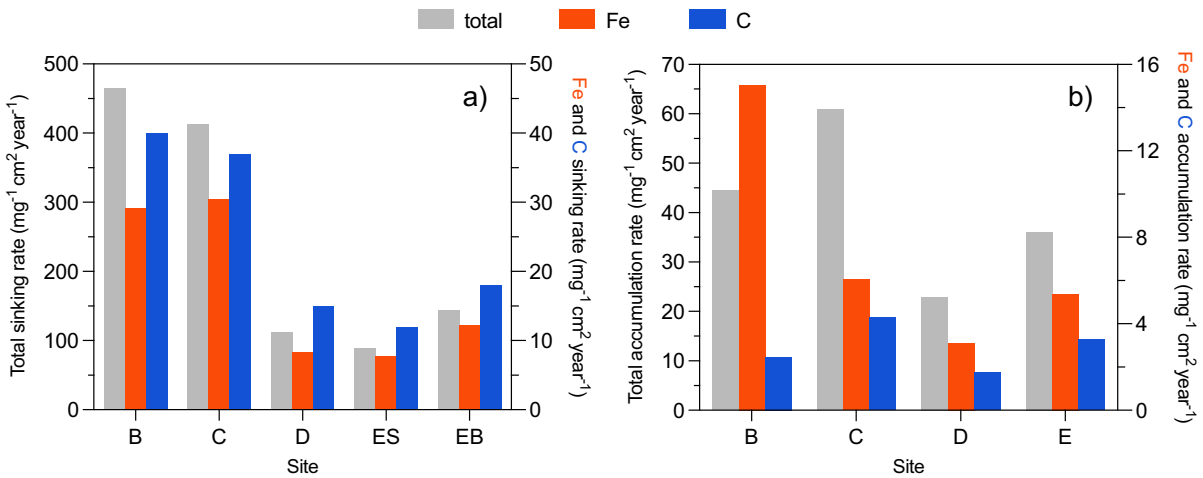

Fig. 4 Sinking rates in sediment traps (panel a) and accumulation rates in sediments (panel b) of total particulate material (left *y*-axes) and the corresponding Fe and C (right *y*-axes) in mg^{-1} cm^2 year^{-1}at the sampling sites. ES and EB sediment traps placed shallow and close to bottom at site E, respectively

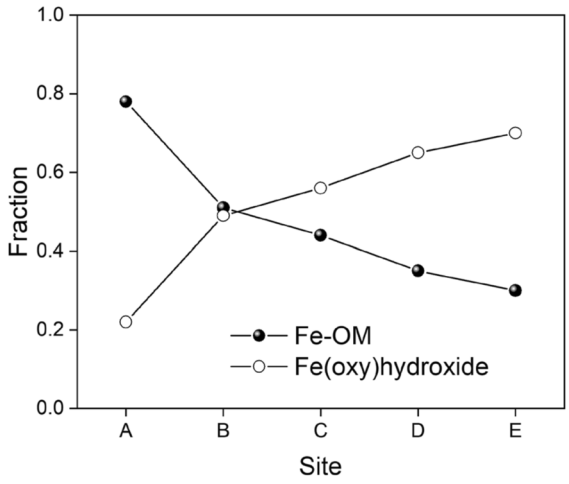

Fig. 5 EXAFS linear combination fitting (LCF) results of the winter surface water samples of Sampling sites: A—inlet (river), B, C, D, E (lake). Only organically complexed (Fe–OM) and Fe(oxy)hydroxide showed a significant contribution and only components with > 5% were included in the LCF analysis

Table 2 Fractions of Fe speciation from the LCF analysis of the sediment trap samples of all lake site

Trap	B	C	D	ES	EB
Fe–OM	0.00	0.00	0.00	0.00	0.00
Fe(oxy)hydroxides*	0.88	0.79	0.80	0.74	0.75
Phyllo-/inosilicates	0.12	0.21	0.20	0.26	0.25
Chi square	76.7	39.0	72.3	46.6	39.0

At site E there was one trap at 7 m depth (ES) and one trap 1.5 m above the sediment (EB). All components with a contribution of < 0.05 were excluded and no Fe-OM was detected in sediment trap samples. *The Fe(oxy)hydroxide fraction for the sediment trap data was entirely made of Ferrihydrite

column declined markedly, and the contribution of Fe(oxy)hydroxide increased (Fig. 5). This pattern was observed for both surface and bottom waters, and no significant difference in Fe speciation between surface and bottom waters was seen ($t_4 = 0.43$; $p = 0.693$). Further, LCF analysis showed no significant contribution of phyllosilicates or inosilicate (Table S4). In contrast, during the summer sampling, Fe(oxy) hydroxides dominated both the inlet and and lake water throughout the the entire lake gradient, as confirmed by LCF analysis of both XANES and EXAFS data (Table S4).

In the settling material collected in sediment traps during the summer (samples were only collected in summer), Fe(oxy)hydroxides were the dominant fraction, with a minor contribution from Fe-containing phyllosilicates/inosilicates and no detectable Fe–OM (Table 2). The contribution of Fe(oxy)hydroxide was largest at site B and decreased slightly with increasing distance from the inlet. Furthermore, samples from the two traps at site E (oxic and the hypoxic conditions) were identical.

Fe speciation in the surface sediments sampled in summer was similar to that in the sinking material collected in traps, with Fe(oxy)hydroxides as the dominant phase and a small contribution of Fe containing phyllo- and inosilicates (Table 3). In surface sediments sampled in winter, only Fe(oxy)hydroxides were detected at site B, whereas at site E an additional contribution of phyllo- and inosilicates and a minor fraction of Fe–OM were identified (Table 3). A change from more crystalline Fe(oxy)hydroxide phases towards more amorphous Fe(oxy)hydroxide phases was found with increasing distance from the inlet, in both winter and summer sediment samples (Table S5).

Table 3 Fractions of Fe speciation from the LCF analysis of the winter and summer sediment samples

Sediment	Winter	B	E	Summer	B	C	D	E
Fe–OM		0.00	0.00		0.00	0.00	0.00	0.09
Fe(oxy)hydroxides*		1.00	0.63		0.86	0.75	0.79	0.72
Phyllo-/inosilicates		0.00	0.37		0.14	0.25	0.21	0.28
Chi square		29.9	61.7		55.2	78.7	45.9	45.9

All components with a contribution of < 0.05 were excluded. *The Fe(oxy)hydroxide fraction includes the sum of Ferrihydrite, Lepidocrocite, and Goethite. For detailed results, see Table S5

OM characterisation

All DRIFT IR spectra of water samples from winter and summer showed carbohydrate bands (between ca. 1000 and 1250 cm^{-1}) and two bands representing carboxyl symmetric and asymmetric stretching centred around 1420 and 1600 cm^{-1} (Table S6) (Niemeyer et al. 1992; Silverstein and Bassler 1962). The ratio between carbohydrate to carboxylate bands increased from A to E. No differences between surface and bottom waters were seen in either summer or winter samples. The aromatic C=C stretch intensity at 1515 cm^{-1} was higher in D and E, and these samples displayed a more pronounced peak at 861 cm^{-1} (CH out of plane deformation in aromatics). The DRIFT IR spectra from site A and B differed between summer and winter (Fig. S1), i.e., the bands at 861 and 1515 cm^{-1} representing aromaticity were slightly more pronounced in summer sampling.

The DRIFT IR spectra of the sinking material and the surface sediment were similar among all sites (Figs. S2 and S3) and showed aliphatic CH_2 stretching at 2927/2854 cm^{-1}, broad bands corresponding to carbohydrates and amide at around 1650 and 1540 cm^{-1}. Only the sediment samples at site B differed from sediments collected at the other sites in the lake (Fig. S3). For site B a broad band centred around 3180 cm^{-1} that may indicate higher contribution of unsaturated C=C–H and/or aromatic rings and the aliphatic signal from CH_2/CH_3 was lower than the other sites.

When comparing to OM in the water column, the aliphatic CH_2 stretching signal (at 2927/2856 cm^{-1}) was higher in settling material and surface sediments (Fig. 6). Moreover, the ratio of carbohydrate to carboxylate was much higher in settling material and

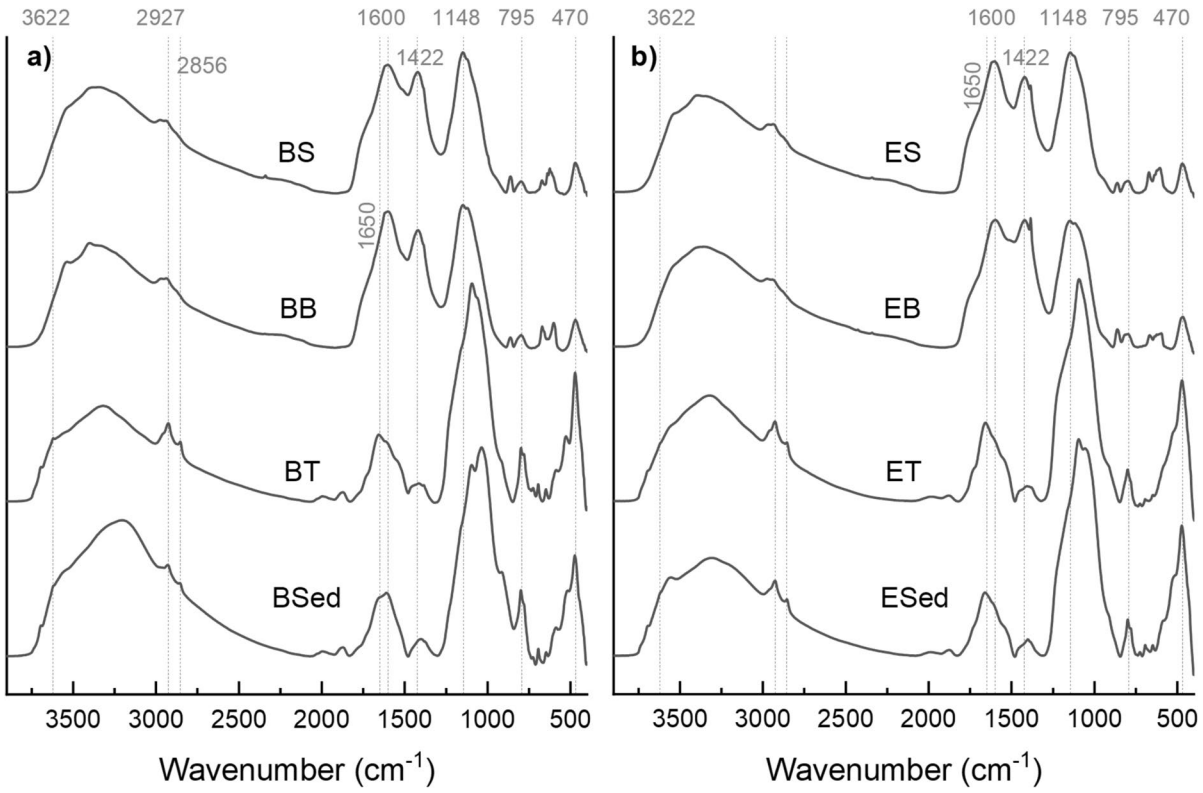

Fig. 6 DRIFT IR spectra of summer samples from site B (left) and site E (right) of surface water (BS and ES) and bottom water (BB and EB) samples, sediment trap samples (BT and ET) and surface sediment samples (BSed and ESed) from. Data from site C and D show the same trends (Figs. S1, S2 and S3). Tentative peak assignments are present in Table S6 and the assigned wavenumbers are for guidance

sediments than in the water phase among all lake sites. Thus, the settling material and sediments contained less carboxyl-rich compounds than water samples but were instead enriched in aliphatic, amide and clay moieties. Further, compared to the water samples, the peak at 1148 cm^{-1} was shifted towards lower wavenumbers (ca. 1035 cm^{-1}) in sinking material and surface sediments, indicating an interference with minerals, namely with Si–O stretching vibrations. The presence of silicates was confirmed by the stronger band at 470 cm^{-1} (Figs. 6 and S3), which is due to the bending mode of Si–O–Si. The bands at 3695 and 3622 cm^{-1} are from OH stretching and indicate the presence of kaolinite and montmorillonite domains, respectively (Bertaux et al. 1998; Madejová et al. 2017).

The high-resolution ^{1}H NMR spectra of water samples looked all very similar and showed the majority of hydrogen signals in aliphatic and carbohydrate regions (from 0.5 to 4.5 ppm; Figs. S4 and S5), in line with the ^{13}C NMR results (see Supporting information section S5 ^{13}C CP-MAS NMR Figs. S6 and S7). The spectra being similar also indicate that the freeze-dried material in all cases were properly redispersed. The spectra contained broad resonances and sharp peaks (i.e. low molecular weight acids) (Simpson et al. 2011; Wilson 1981). Several sharp peaks were identified at 0.06, 1.83, 3.26 and 8.35 ppm, corresponding to silicate, acetic acid, methanol and formic acid, respectively (Whitty et al. 2021). The spectra of ^{1}H NMR were divided into six regions as indicated in Fig. S5, corresponding to different chemical environment of hydrogens (aliphatic region 1, 2 and 3; carbohydrate region 4; and aromatic region 5 and 6). All surface water samples were very similar with essentially no difference in the relative intensity distribution (Fig. 7).

Discussion

By sampling across a spatial gradient in Lake Bolmen—starting from the main inlet and continuing offshore into the lake—we wanted to understand how interactions between Fe and OM vary and influence fluxes, particularly from the water column to the sediments. As hypothesized, Fe and OM concentrations decreased with increasing distance from the inlet, and during winter sampling the contribution of Fe–OM decreased and the Fe(oxy)hydroxide fraction increased along the same gradient. However, during summer sampling Fe(oxy)hydroxides

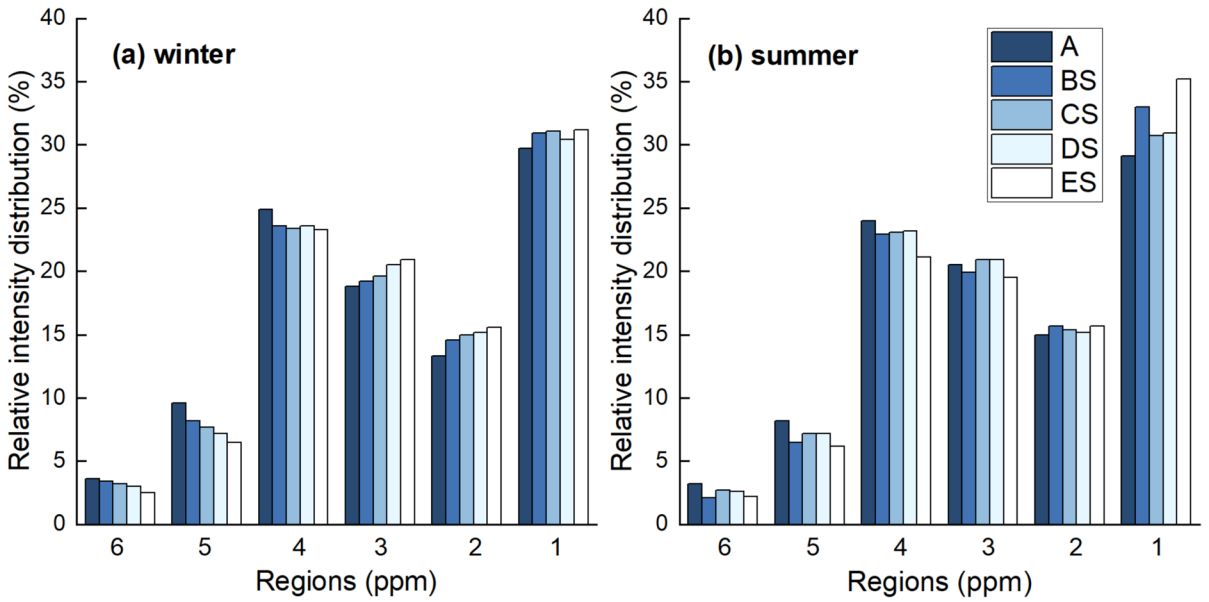

Fig. 7 Comparison of ^{1}H NMR area integrals over six regions (aromatic region 6 and 5; carbohydrates region 4 and aliphatic region 3, 2 and 1) of the spectra from winter (**a**) and summer (**b**) surface water samples. The regions' areas are presented as % of the total area

were dominating both in the inlet and lake water. Also, in line with our predictions, Fe(oxy)hydroxides were dominant in sinking material and surface sediments suggesting preferential loss. Interestingly, there was a similar preferential sedimentation of aliphatic OM. It is currently unknown whether mineral and aliphatic OM co-aggregate or sediment individually. The possible fate of OM and its interactions with Fe(oxy)hydroxides is further discussed below.

Flow-related variation in Fe and OM entering from the inlet

High flow-conditions during winter-sampling, and low-flow conditions during summer sampling seemed to cause distinct differences in Fe and OM entering from the inlet stream. Fe and OM concentrations (TOC) were higher in winter and mononuclear organic Fe–OM was the dominant Fe phase. The high precipitation and wet conditions which preceded the winter sampling promote a stronger hydrological connectivity between streams and organic surface soils, which has been shown to increase mobilization of Fe–OM from organic-rich soil layers to adjacent surface waters (Dahlqvist et al. 2007; Sundman et al. 2014; Herzog et al. 2020). The high OM concentration and low pH that prevail in organic soil layers favour organic complexation (Neubauer et al. 2013; Liu and Millero 2002; Herzog et al. 2020).

In summer Fe concentrations were lower and the Fe was predominantly composed of Fe(oxy)hydroxides. During drier conditions, such as observed during summer sampling, flow-paths run through deeper soil layers, which in coniferous forest mineral soils have a considerably lower OM content and a higher pH. Iron from these deeper flow-paths are therefore more likely to enter the stream as Fe(oxy)hydroxides, or Fe(II) which may rapidly hydrolyse and form Fe(oxy)hydroxides during mixing with oxic stream water (Vasyukova et al. 2010). A dominance of Fe(oxy)hydroxides under summer low-flow conditions, and increasing contribution of Fe–OM under wet conditions in winter, have been observed previously for Storån (Björnerås et al. 2021), and in rivers draining similar landscapes (Herzog et al. 2020).

OM in the inlet was predominantly from terrestrial sources during both winter and summer, supported by $\delta^{13}C$ and E2:E4 ratios (Weishaar et al. 2003; Lajtha and Michener 1994; Ilina et al. 2014). The presence of carbohydrates and aromatics, as indicated by DRIFT IR and NMR analysis, suggested that the OM originated from decomposing terrestrial vascular plants rich in lignin-derived unsaturated material and phenolic compounds (Thurman 2012; Tranvik 1998). The OM showed a high level of aromaticity in both winter and summer, supported by high SUVA values, although the DRIFT IR and NMR revealed subtle differences suggesting a higher contribution of aromatics and phenolic compounds during summer. This may be attributed to a greater input of OM from peat soils rather than forest soils during periods of low-flow (Ågren et al. 2008).

Fe and OM fluxes along the spatial gradient

As hypothesized, concentrations of Fe and OM (TOC) in the water column declined with increasing distance from the inlet. The loss of Fe and OM from the water column was probably related to the increasing water residence time in the lake, providing critical time for physical and biogeochemical processes to take place (Weyhenmeyer et al. 2014). The declining concentrations of Fe and OM along the spatial gradient coincided with higher sinking and accumulation rates of Fe and OM closer to the inlet probably influenced by the river plume (Piton et al. 2022) in comparison to the more offshore sites, where lake hydrodynamics may have become the dominant factor influencing particle behavior (Davison 1993). These results support that downward sinking is a significant loss process for riverine Fe and OM in the lake. For Fe, sinking is the only route out of the water column, and as water movements slow down with longer residence time, larger and more crystalline Fe phases, as seen in site B, may be lost first (Davison 1993). Like Fe, the loss of OM from the water column could be attributed to aggregation and sinking, potentially in association with Fe (Wilkinson et al. 1997; Mikutta et al. 2008). The high Fe:OC molar ratio in the sinking material (0.12–0.18) may suggest that Fe acts as a vector for downward transport of OM (Mikutta et al. 2014). However, unlike Fe, OM loss can also be caused by photochemical transformations and microbial remineralization, which may be closely linked as the former can stimulate the latter (Allesson et al. 2021; Vähätalo et al. 2003). Thus, the loss of OM from the water column observed here and in previous

studies (Teodoru et al. 2013; Tranvik et al. 2009), was driven by downward sinking partially, but not entirely.

Links between Fe speciation and fluxes

Fe speciation differed between the times of sampling, along the spatial gradient and between sample types, i.e. water column, sinking material and surface sediments. The decreasing contribution of Fe–OM in the water column, and the absence of Fe–OM in settling material, supports the hypothesis that Fe–OM is transformed into Fe(oxy)hydroxides along the spatial gradient in the lake. Furthermore, since Fe(oxy)hydroxides were strongly dominant in the settling material, these results are in line with the prediction that Fe(oxy)hydroxides should be preferentially lost from the water column by precipitation and sinking to sediments (Björnerås et al. 2021).

While Fe speciation was similar across the sediment traps in all sites, surface sediments of the lake showed some spatial variation. A higher contribution of Fe with a more defined crystalline structure (goethite) was found in sediments close the inlet (site B) than in the downstream sediments. This may reflect that larger and more thermodynamically stable minerogenic phases settle faster when velocity is reduced as the stream water enters the lake (Filella et al. 1993). Another possibility is that particle transport occurs through horizontal advective flow within the river and carries particles into the lake (Lemmin and Imboden 1987). The composition of sediments closer to the inlet may therefore be more directly influenced by the river plume and the associated riverine sediment loads, which is consistent with the higher sediment accumulation rates observed near the inlet (Davison 1993; Piton et al. 2022).

As discussed above, the Fe speciation of sediments may be influenced by riverine supply and processes in the water column, but also by in situ transformations within the sediments (Engstrom and Wright 1984; Lemmin and Imboden 1987). Reducing conditions may promote release of Fe(II) from sediments, and bottom current mobilization followed by Fe(oxy)hydroxides precipitation may promote lateral transport (“shuttling”), which could be an additional source for the amorphous Fe(oxy) hydroxide phases found at deeper sites further away from the inlet (Davison 1993). Slightly elevated Fe concentrations in the hypoxic bottom water at the deepest site (E) during summer suggest that reducing conditions may promote the dissolution and resuspension of Fe from sediments (Davison 1993; Lenstra et al. 2021). However, since anoxic conditions in the water column are only found in the deepest areas of Lake Bolmen (Björnerås et al. 2021), Fe translocation due to reductive dissolution is likely limited to these areas.

Links between OM composition and fluxes

We observed differences in OM composition in the water column along the spatial gradient. With increasing distance from the inlet, a relative decrease in the proportion of aromatic compounds, carboxylic acid functionality and average molecular weight of CDOM was observed. Loss of aromaticity and carboxyl groups with increasing residence time has been observed in other studies of freshwater systems (Kellerman et al. 2015) and is in line with our prediction that these should be preferentially removed with sinking aggregates. However, since the settling material and surface sediments were not enriched in aromatic and carboxylate fractions, the loss could not be explained by this process, but more likely by photo induced changes of the OM composition.

Aromatic compounds are known to be highly photo reactive and prone to degrade upon irradiation (Strome and Miller 1978; Stubbins et al. 2010; Helms et al. 2013), and the influence of photodegradation increase with increasing light exposure in the lake and increasing residence time. Moreover, decarboxylation of OM has been found to be a result of photodegradation (Thorn et al. 2010; Xie et al. 2004). Thus, observed structural changes of the OM in the water column could be the result of photodegradation.

The decarboxylation, the loss of aromaticity and increase in aliphatic content which follows photodegradation, result in a more hydrophobic and less soluble OM (Thorn et al. 2010), and thereby promote flocculation and formation of particulate OM (Helms et al. 2013). Photo-induced flocculates have been observed to show an accumulation of amides, suggested to be the result of ammonia that is produced during the photodegradation reacting with esters of the OM to form alkyl amides. Helms et al. (2013). The high contribution of aliphatic compounds and

amides in the sediment traps and surface sediments compared to the water column are therefore also consistent with the impact of photochemical processes. Furthermore, OM of hydrophobic character preferentially adsorbs onto Fe(oxy)hydroxides, due to the density and distribution of surface hydroxyl groups of the latter, which interact with the hydrophobic groups in OM (Gu et al. 1994).

The surface sediments closest to the inlet exhibited higher levels of aromaticity and lower levels of aliphatic compounds. Since photodegradation is likely to have a lesser impact in running waters, the elevated aromaticity in the sediments close to the inlet could be attributed to the affinity between aromatic compounds with high carboxylate functionality and Fe(oxy)hydroxides (Kothawala et al. 2014; Coward et al. 2018). As discussed in the previous section, this discrepancy in sediments at site B may be attributed to the influence of the river plume and the riverine sediment loads, which contain a greater amount of crystalline Fe(oxy)hydroxides which could be associated with the aromatic compounds.

Possible transformation processes in the lake and the role of Fe as a precursor for the fate of OM

The spatial gradients observed for Fe speciation and OM characteristics suggest that transformations occurred within the lake, e.g., aromaticity and carboxyl functionality were lost and Fe–OM was transformed to Fe(oxy)hydroxides. As discussed in the previous section, the structural changes of OM in the water column conform with photo-induced transformations (Stubbins et al. 2010; Hawkes et al. 2016). Solar radiation can also influence the speciation of Fe as well as the interaction between Fe and OM, including processes like photoaggregation (see Gao and Zepp 1998). High energy UV radiation and lower wavelengths of the visual region have the capacity to chemically reduce Fe(III) to Fe(II). This can be direct, by photon absorption and ligand to metal charge transfer (LMCT) where an electron is transferred from the ligand (e.g. carboxylate group) to the Fe(III), and result in decarboxylation and release of Fe(II) (Helms et al. 2013). It can also be indirect, when photolysis of OM produce reactive oxygen species (ROS), such as superoxide ($O_2^{-\cdot}$), hydroxyl radicals ($OH^{\cdot}$), and hydrogen peroxide (H_2O_2), which mediate the reduction of Fe(III) (Southworth and Voelker 2003). Re-oxidation of photo-reduced Fe(II) can also result in formation of ROS (Lueder et al. 2020).The release of Fe from organic complexes, which is the result of all of the above mechanisms, promote formation of Fe(oxy)hydroxide (Kopáček et al. 2006; Gu et al. 2017). The altered OM with reduced complexing capacity constrains the formation of new Fe–OM, and further favors the prevalence of Fe(oxy)hydroxides. Thus, light is likely a strong driver of the transformations of both OM and Fe which are observed along the studied transect in Lake Bolmen.

Apart from photochemical transformation, pH gradients may impact the Fe speciation (Neubauer et al. 2013). An increase in pH, as observed between the inlet stream (5.8) and lake (6.7) at the time for winter sampling, can induce precipitation of mononuclear Fe–OM into Fe(oxy)hydroxides due to strong hydrolytic tendencies and thus a separation of Fe and OM (Lofts et al. 2008; Karlsson and Persson 2012). This may have contributed to the loss of Fe–OM and increasing proportion of Fe(oxy)hydroxides between the inlet stream and site B during winter sampling.

The high levels of amorphous Fe(oxy)hydroxide found in sediment traps and sediments in this study suggest that in-lake formation of Fe(oxy)hydroxide promotes aggregation and the sinking out of the water column (Tipping and Ohnstad 1984). The freshly precipitated Fe may then scavenge significant quantities of OM (Luider et al. 2003). However, counter to our hypothesis—that aromatic organic compounds with a high density of carboxylic groups and high affinity for Fe(oxy)hydroxide would be preferentially removed and dominate in the sediment traps and sediments—the settling material and sediments were enriched in aliphatic compounds. This is in line with a lab study, where photochemically induced flocculates were more aliphatic than the residual dissolved OM (Helms et al. 2013). Our overall interpretation is that flocculation is facilitated by photochemical transformations promoting the formation of amorphous Fe(oxy)hydroxides, and an increasing contribution of aliphatic OM which is hydrophobic and susceptible to adsorption (Vindedahl et al. 2016). The co-precipitation of amorphous Fe(oxy)hydroxide and aliphatic dominated OM may then represent an important mechanism by which newly formed particulate OM is exported to the sediments (Fig. 8).

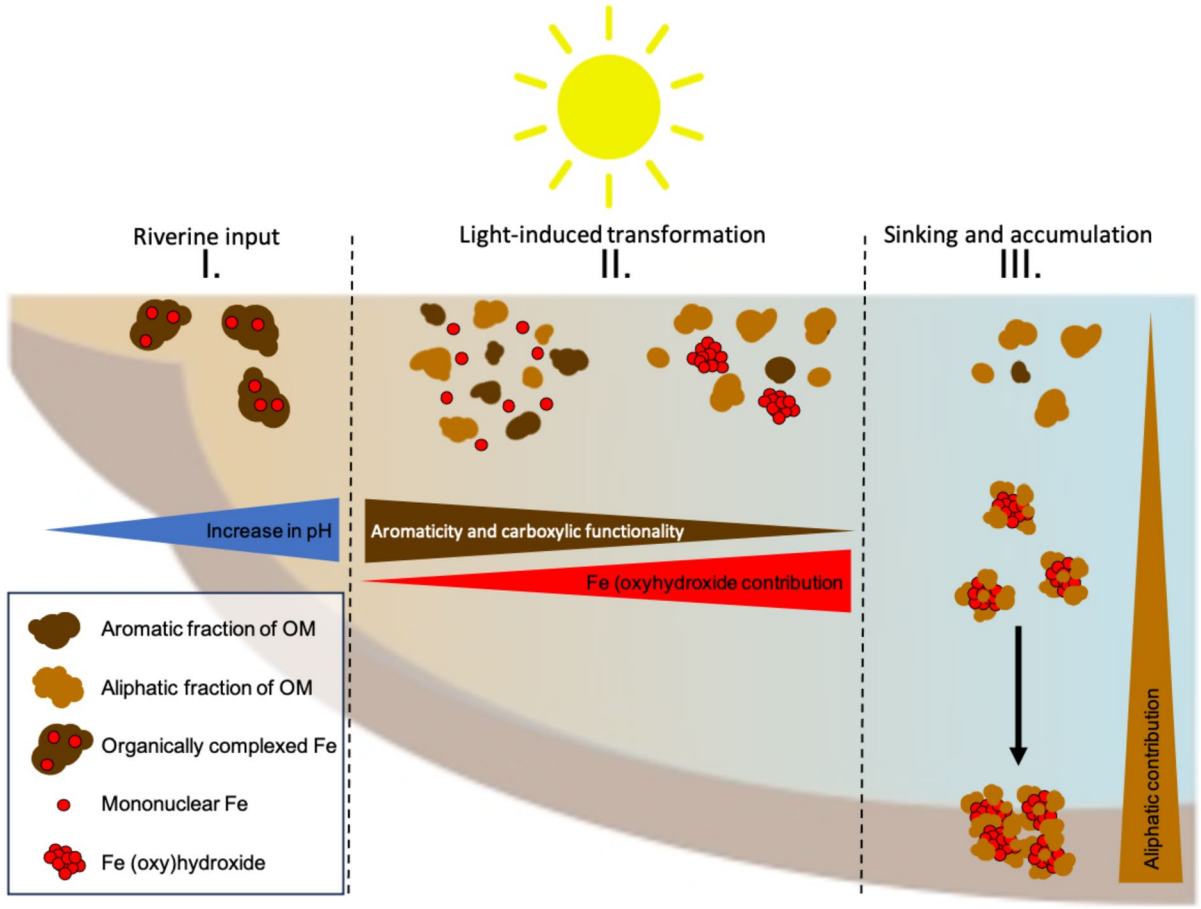

Fig. 8 Proposed mechanisms for light-induced co-precipitation of iron and organic matter in the lake: (I) Input of organically complexed Fe and OM with high aromaticity and carboxylic function and potential pH effect on Fe precipitation; (II) Light-induced transformation of OM in suspension, resulting in loss of aromaticity and carboxylic complexing capacity for Fe. Light can also trigger release of Fe by reduction. Following the release of Fe, colloidal Fe(oxy)hydroxides are formed. (III) The freshly formed Fe(oxy)hydroxides adsorb the most aliphatic fraction of OM and is lost by sinking to the sediment

Conclusion

The aim of this study was to investigate how interactions between Fe and OM affect their biogeochemical cycling in a lake, with a particular focus on understanding the role of Fe as a precursor of aggregation and a vector for OM transfer to the sediments.

Compared to the inlet water, Fe–OM transformed into Fe(oxy)hydroxides and carboxylic functionality of the OM in the water phase was lost with increasing distance from the inlet. Settling material and surface sediments were dominated by Fe(oxy)hydroxides, presumably in association with predominantly aliphatic carbon and amides. This leads us to propose that photo-induced changes in Fe speciation and OM composition may prime Fe to act as a precursor for aggregation and sedimentation of Fe and aliphatic dominated OM. This is a relevant finding in light of increasing Fe concentrations in northern regions (Björnerås et al. 2017) and given that inland water sediments accumulate three times more OC annually then marine sediments globally (Drake et al. 2018).

This study demonstrates the utility of combining multiple advanced techniques for Fe and OM characterization, coupled with relevant ancillary data, to study interactions across a continuum from source (inlet) through lake water column to sink (lake sediment). However, it's important to note that these results provide a snapshot from a single boreal lake at two time points in an inherently temporally dynamic

system. To fully understand the significance of light-induced transformations of Fe and OM, further investigations should account for temporal variations, including seasonal changes in light period and intensity, hydrological flowpaths within the catchment, and lake stratification patterns. A range of lake types should also be studied to reveal the generality of these processes. The impact of climate change on hydrology and Fe and OM fluxes into surface waters in boreal regions (Björneråas et al. 2017; Haaland et al. 2010), raises the question how climate-driven hydrological shifts may influence light-induced transformations and sedimentation processes in boreal lakes. Additionally, experimental work is required to establish firm links between observed spatial patterns and the underlying processes and mechanisms. Expanding the scope of research in these directions will enhance our knowledge of Fe and OM dynamics in lakes and their response to environmental factors. Ultimately, this can yield valuable insights for the predictive modeling and management of carbon cycling and storage in lakes, and a more comprehensive understanding of global carbon cycling mechanisms.

Acknowledgments and Funding The Swedish Research Council (Dnr: 2023-04740, 2020-04293 and 2016-04561), the Swedish strategic research area Biodiversity and Ecosystem Services in a Changing Climate (BECC) and the Knut & Alice Wallenberg Foundation (2013.0073). supported this work. Synchrotron work was conducted at beamline line 4–1 at the Stanford Synchrotron Radiation Lightsource (SSRL), California, USA. Use of the Stanford Synchrotron Radiation Lightsource, SLAC National Accelerator Laboratory, is supported by the U.S. Department of Energy, Office of Science, Office of Basic Energy Sciences under Contract No. DE-AC02-76SF00515. The SSRL Structural Molecular Biology Program is supported by the DOE Office of Biological and Environmental Research, and by the National Institutes of Health, National Institute of General Medical Sciences (including P41GM103393). The contents of this publication are solely the responsibility of the authors and do not necessarily represent the official views of NIGMS or NIH. We also acknowledge MAX IV Laboratory for time on Beamline Balder under Proposal 20211248, 20200836 and 20200018 and the support by beamline scientist Susan Nehzati. Research conducted at MAX IV, a Swedish national user facility, is supported by the Swedish Research council under contract 2018-07152, the Swedish Governmental Agency for Innovation Systems under contract 2018-04969, and Formas under contract 2019-02496.

Author's contributions E.S.K. developed the idea for this study. S.D.H., and M.S. coordinated the sampling efforts, and S.D.H., M.S, and V.M. collected, analysed the data and wrote the manuscript with E.S.K., U.O. and P.P. provided substantial intellectual contribution to the data analysis and commented on the manuscript.

Funding Open access funding provided by Roskilde University.

Data Availability The XAS data set can be downloaded from the repository Zenodo (https://doi.org/10.5281/zenodo.13918639).

Declarations

Conflict of interest The authors have no relevant financial or non-financial interests to disclose.

References

Ågren A, Buffam I, Berggren M, Bishop K, Jansson M, Laudon H (2008) Dissolved organic carbon characteristics in boreal streams in a forest-wetland gradient during the transition between winter and summer. J Geophys Res Biogeosci 113(G3).

Allesson L, Koehler B, Thrane JE, Andersen T, Hessen DO (2021) The role of photomineralization for CO emissions in boreal lakes along a gradient of dissolved organic matter. Limnol Oceanogr 66(1):158–170

Barber A, Brandes J, Leri A, Lalonde K, Balind K, Wirick S, Wang J, Gélinas Y (2017) Preservation of organic matter in marine sediments by inner-sphere interactions with reactive iron. Sci Rep 7(1):1–10

Bertaux J, Froehlich F, Ildefonse P (1998) Multicomponent analysis of FTIR spectra; quantification of amorphous and crystallized mineral phases in synthetic and natural sediments. J Sediment Res 68(3):440–447

Björneråas C, Weyhenmeyer GA, Evans CD, Gessner MO, Grossart HP, Kangur K, et al (2017). Widespread increases in iron concentration in European and North American freshwaters. Global Biogeochem Cycles 31(10):1488–1500.

Björnerås C, Persson P, Weyhenmeyer GA, Hammarlund D, Kritzberg ES (2021) The lake as an iron sink-new insights on the role of iron speciation. Chem Geol, 120529.

Blazevic A, Orlowska E, Kandioller W, Jirsa F, Keppler BK, Tafili-Kryeziu M, Linert W, Krachler RF, Krachler R, Rompel A (2016) Photoreduction of terrigenous Fe-humic substances leads to bioavailable iron in oceans. Angew Chem 128(22):6527–6532

Coward EK, Ohno T, Plante AF (2018) Adsorption and molecular fractionation of dissolved organic matter on iron-bearing mineral matrices of varying crystallinity. Environ Sci Technol 52(3):1036–1044

Dahlqvist R, Andersson K, Ingri J, Larsson T, Stolpe B, Turner D (2007) Temporal variations of colloidal carrier phases and associated trace elements in a boreal river. Geochim Cosmochim Acta 71(22):5339–5354

Davison W (1993) Iron and manganese in lakes. Earth Sci Rev 34(2):119–163

De Haan H, De Boer T (1987) Applicability of light absorbance and fluorescence as measures of concentration and molecular size of dissolved organic carbon in humic Lake Tjeukemeer. Water Res 21(6):731–734

Drake TW, Raymond PA, Spencer RG (2018) Terrestrial carbon inputs to inland waters: a current synthesis of estimates and uncertainty. Limnol Oceanogr Lett 3(3):132–142

Drozdova OY, Aleshina A, Tikhonov V, Lapitskiy S, Pokrovsky O (2020) Coagulation of organo-mineral colloids and formation of low molecular weight organic and metal complexes in boreal humic river water under UV-irradiation. Chemosphere 250:126216

Engstrom D, Wright H (1984) Lake sediments and environmental history. Studies in palaeoecolology in honour of Winifred Tutin. University of Minnesota Press, Minneapolis, pp 11–63.

Filella M, Buffle J, Leppard GG (1993) Characterization of submicrometre colloids in freshwaters: evidence for their bridging by organic structures. Water Sci Technol 27(11):91

Gao H, Zepp RG (1998) Factors influencing photoreactions of dissolved organic matter in a coastal river of the southeastern United States. Environ Sci Technol 32(19):2940–2946

Gu B, Schmitt J, Chen Z, Liang L, McCarthy JF (1994) Adsorption and desorption of natural organic matter on iron oxide: mechanisms and models. Environ Sci Technol 28(1):38–46

Gu Y, Lensu A, Perämäki S, Ojala A, Vähätalo AV (2017) Iron and pH regulating the photochemical mineralization of dissolved organic carbon. ACS Omega 2(5):1905–1914

Guillemette F, von Wachenfeldt E, Kothawala DN, Bastviken D, Tranvik LJ (2017) Preferential sequestration of terrestrial organic matter in boreal lake sediments. J Geophys Res Biogeosci 122(4):863–874

Haaland S, Hongve D, Laudon H, Riise G, Vogt R (2010) Quantifying the drivers of the increasing colored organic matter in boreal surface waters. Environ Sci Technol 44(8):2975–2980

Hassellöv M, Lyvén B, Haraldsson C, Sirinawin W (1999) Determination of continuous size and trace element distribution of colloidal material in natural water by on-line coupling of flow field-flow fractionation with ICPMS. Anal Chem 71(16):3497–3502

Hawkes JA, Dittmar T, Patriarca C, Tranvik L, Bergquist J (2016) Evaluation of the Orbitrap mass spectrometer for the molecular fingerprinting analysis of natural dissolved organic matter. Anal Chem 88(15):7698–7704

Helms JR, Stubbins A, Ritchie JD, Minor EC, Kieber DJ, Mopper K (2008) Absorption spectral slopes and slope ratios as indicators of molecular weight, source, and photobleaching of chromophoric dissolved organic matter. Limnol Oceanogr 53(3):955–969. https://doi.org/10.4319/lo.2008.53.3.0955

Helms JR, Mao J, Schmidt-Rohr K, Abdulla H, Mopper K (2013) Photochemical flocculation of terrestrial dissolved organic matter and iron. Geochim Cosmochim Acta 121:398–413

Hertkorn N, Benner R, Frommberger M, Schmitt-Kopplin P, Witt M, Kaiser K, Kettrup A, Hedges JI (2006) Characterization of a major refractory component of marine dissolved organic matter. Geochim Cosmochim Acta 70(12):2990–3010

Herzog SD, Conrad S, Ingri J, Persson P, Kritzberg ES (2019) Spring flood induced shifts in Fe speciation and fate at increased salinity. Appl Geochem 109:104385. https://doi.org/10.1016/j.apgeochem.2019.104385

Herzog SD, Persson P, Kritzberg ES (2017) Salinity effects on iron speciation in boreal river waters. Environ Sci Technol 51(17):9747–9755

Herzog SD, Persson P, Kvashnina K, Kritzberg ES (2020) Organic iron complexes enhance iron transport capacity along estuarine salinity gradients of Baltic estuaries. Biogeosciences 17(2):331–344

Hwang T-L, Shaka A (1995) Water suppression that works. Excitation sculpting using arbitrary wave-forms and pulsed-field gradients. J Magn Resonan Ser A 112(2):275–279.

Ilina SM, Drozdova OY, Lapitskiy SA, Alekhin YV, Demin VV, Zavgorodnyaya YA, Shirokova LS, Viers J, Pokrovsky OS (2014) Size fractionation and optical properties of dissolved organic matter in the continuum soil solution-bog-river and terminal lake of a boreal watershed. Org Geochem 66:14–24.https://doi.org/10.1016/j.orggeochem.2013.10.008

Karlsson T, Persson P (2012) Complexes with aquatic organic matter suppress hydrolysis and precipitation of Fe(III). Chem Geol 322–323:19–27. https://doi.org/10.1016/j.chemgeo.2012.06.003

Karlsson T, Persson P, Skyllberg U, Mörth C-M, Giesler R (2008) Characterization of iron (III) in organic soils using extended X-ray absorption fine structure spectroscopy. Environ Sci Technol 42(15):5449–5454

Kellerman AM, Kothawala DN, Dittmar T, Tranvik LJ (2015) Persistence of dissolved organic matter in lakes related to its molecular characteristics. Nat Geosci 8(6):454–457

Kleber M, Eusterhues K, Keiluweit M, Mikutta C, Mikutta R, Nico PS (2015) Mineral–organic associations: formation, properties, and relevance in soil environments. Adv Agron 130:1–140

Klementiev K (2000) VIPER for Windows (Visual Processing in EXAFS Researches), freeware.

Köhler SJ, Kothawala D, Futter MN, Liungman O, Tranvik L (2013) In-lake processes offset increased terrestrial inputs of dissolved organic carbon and color to lakes. PLoS ONE 8(8):e70598

Kopáček J, Marešová M, Norton SA, Porcal P, Veselý J (2006) Photochemical source of metals for sediments. Environ Sci Technol 40(14):4455–4459

Kothawala DN, Stedmon CA, Müller RA, Weyhenmeyer GA, Köhler SJ, Tranvik LJ (2014) Controls of dissolved organic matter quality: Evidence from a large-scale boreal lake survey. Glob Change Biol 20(4):1101–1114

Kritzberg ES, Ekstrom SM (2012) Increasing iron concentrations in surface waters—a factor behind brownification? Biogeosciences 9(4):1465–1478. https://doi.org/10.5194/bg-9-1465-2012

Lajtha K, Michener RH (1994) Stable isotopes in ecology and environmental science. Blackwell Scientific Publications, New York.

Lalonde K, Mucci A, Ouellet A, Gélinas Y (2012) Preservation of organic matter in sediments promoted by iron. Nature 483(7388):198–200

Larsen S, Andersen T, Hessen DO (2011) Climate change predicted to cause severe increase of organic carbon in lakes. Glob Change Biol 17(2):1186–1192

Lemmin U, Imboden D (1987) Dynamics of bottom currents in a small lake 1. Limnol Oceanogr 32(1):62–75

Lenstra WK, Hermans M, Séguret MJ, Witbaard R, Severmann S, Behrends T, Slomp CP (2021) Coastal hypoxia and eutrophication as key controls on benthic release and water column dynamics of iron and manganese. Limnol Oceanogr 66(3):807–826

Lindström G, Bartosova A, Hjerdt N, Strömqvist J (2018) Uppehållstider i ytvatten i relation tillvattenkvalitetNET, ett generellt uppskalningsverktyg.

Liu X, Millero FJ (2002) The solubility of iron in seawater. Mar Chem 77(1):43–54

Lofts S, Tipping E, Hamilton-Taylor J (2008) The chemical speciation of Fe (III) in freshwaters. Aquat Geochem 14(4):337–358

Lueder U, Jørgensen BB, Kappler A, Schmidt C (2020) Photochemistry of iron in aquatic environments. Environ Sci Process Impacts 22(1):12–24

Luider C, Petticrew E, Curtis P (2003) Scavenging of dissolved organic matter (DOM) by amorphous iron hydroxide particles Fe (OH) 3 (s). Hydrobiologia 494:37–41

Lyvén B, Hassellöv M, Turner DR, Haraldsson C, Andersson K (2003) Competition between iron-and carbon-based colloidal carriers for trace metals in a freshwater assessed using flow field-flow fractionation coupled to ICPMS. Geochim Cosmochim Acta 67(20):3791–3802

Madejová J, Gates W, Petit S (2017) IR spectra of clay minerals. Developments in clay science, Vol. 8, pp. 107–149. Elsevier, Amsterdam.

Massicotte P, Markager S (2016) Using a Gaussian decomposition approach to model absorption spectra of chromophoric dissolved organic matter. Mar Chem 180:24–32

Mikutta C, Mikutta R, Bonneville S, Wagner F, Voegelin A, Christl I, Kretzschmar R (2008) Synthetic coprecipitates of exopolysaccharides and ferrihydrite. Part I: Characterization. Geochim Cosmochim Acta 72(4):1111–1127.

Mikutta R, Lorenz D, Guggenberger G, Haumaier L, Freund A (2014) Properties and reactivity of Fe-organic matter associations formed by coprecipitation versus adsorption: Clues from arsenate batch adsorption. Geochim Cosmochim Acta 144:258–276

Monteith DT, Stoddard JL, Evans CD, De Wit HA, Forsius M, Høgåsen T et al (2007) Dissolved organic carbon trends resulting from changes in atmospheric deposition chemistry. Nature 450(7169):537–540.

Neubauer E, Kohler SJ, von der Kammer F, Laudon H, Hofmann T (2013) Effect of pH and stream order on iron and arsenic speciation in boreal catchments. Environ Sci Technol 47(13):7120–7128. https://doi.org/10.1021/es401193j

Niemeyer J, Chen Y, Bollag JM (1992) Characterization of humic acids, composts, and peat by diffuse reflectance Fourier-transform infrared spectroscopy. Soil Sci Soc Am J 56(1):135–140

Piton V, Soulignac F, Lemmin U, Graf B, Wynn HK, Blanckaert K, Barry DA (2022) Tracing unconfined nearfield spreading of a river plume interflow in a large Lake (Lake Geneva): hydrodynamics, suspended particulate matter, and associated fluxes. Front Water 4:943242

Porcal P, Dillon PJ, Molot LA (2013) Photochemical production and decomposition of particulate organic carbon in a freshwater stream. Aquat Sci 75(4):469–482

Renberg I, Hansson H (2008) The HTH sediment corer. J Paleolimnol 40:655–659

Sarkkola S, Nieminen M, Koivusalo H, Laurén A, Kortelainen P, Mattsson T, Palviainen M, Piirainen S, Starr M, Finér L (2013) Iron concentrations are increasing in surface waters from forested headwater catchments in eastern Finland. Sci Total Environ 463–464:683–689. https://doi.org/10.1016/j.scitotenv.2013.06.072

Shapiro J (1966) On the measurement of ferrous Iron in Natural WATERS1. Limnol Oceanogr 11(2):293–298

Silverstein RM, Bassler GC (1962) Spectrometric identification of organic compounds. J Chem Educ 39(11):546

Simpson AJ, McNally DJ, Simpson MJ (2011) NMR spectroscopy in environmental research: from molecular interactions to global processes. Prog Nucl Magn Reson Spectrosc 58(3–4):97–175

Southworth BA, Voelker BM (2003) Hydroxyl radical production via the photo-Fenton reaction in the presence of fulvic acid. Environ Sci Technol 37(6):1130–1136

Spadini L, Bott M, Wehrli B, Manceau A (2003) Analysis of the major Fe bearing mineral phases in recent lake sediments by EXAFS spectroscopy. Aquat Geochem 9(1):1–17

SS-28311 (2017) Soil analysis—determination of trace elements in soil by extraction with nitric acid. Swedish Standards Institute, Stockholm.

Strome DJ, Miller MC (1978) Photolytic changes in dissolved humic substances: With 3 figures and 2 tables in the text. Internationale Vereinigung Theoretische Angewandte Limnologie: Verhandlungen 20(2):1248–1254

Stubbins A, Spencer RG, Chen H, Hatcher PG, Mopper K, Hernes PJ, Mwamba VL, Mangangu AM, Wabakanghanz JN, Six J (2010) Illuminated darkness: molecular signatures of Congo River dissolved organic matter and its photochemical alteration as revealed by ultrahigh precision mass spectrometry. Limnol Oceanogr 55(4):1467–1477

Sun J, Mailloux BJ, Chillrud SN, van Geen A, Thompson A, Bostick BC (2018) Simultaneously quantifying ferrihydrite and goethite in natural sediments using the method of standard additions with X-ray absorption spectroscopy. Chem Geol 476:248–259

Sundman A, Karlsson T, Persson P (2013) An experimental protocol for structural characterization of Fe in dilute natural waters. Environ Sci Technol 47(15):8557–8564. https://doi.org/10.1021/es304630a

Sundman A, Karlsson T, Laudon H, Persson P (2014) XAS study of iron speciation in soils and waters from a boreal catchment. Chem Geol 364:93–102. https://doi.org/10.1016/j.chemgeo.2013.11.023

Teodoru CR, Del Giorgio PA, Prairie YT, St-Pierre A (2013) Depositional fluxes and sources of particulate carbon and nitrogen in natural lakes and a young boreal reservoir in Northern Québec. Biogeochemistry 113:323–339

Thorn KA, Younger SJ, Cox LG (2010) Order of functionality loss during photodegradation of aquatic humic substances. J Environ Qual 39(4):1416–1428

Thurman EM (2012) Organic geochemistry of natural waters, vol. 2. Springer, Cham.

Tipping E, Ohnstad M (1984) Colloid stability of iron oxide particles from a freshwater lake. Nature 308(5956):266–268

Tranvik LJ (1998) Degradation of dissolved organic matter in humic waters by bacteria *Aquatic humic substances* Springer, Cham, pp. 259–283

Tranvik LJ, Downing JA, Cotner JB, Loiselle SA, Striegl RG, Ballatore TJ et al. (2009) Lakes and reservoirs as regulators of carbon cycling and climate. Limnol Oceanogr 54(6part2):2298–2314.

Vähätalo AV, Salonen K, Münster U, Järvinen M, Wetzel RG (2003) Photochemical transformation of allochthonous organic matter provides bioavailable nutrients in a humic lake. Arch Hydrobiol 156(2):287–314

Vasyukova E, Pokrovsky O, Viers J, Oliva P, Dupré B, Martin F, Candaudap F (2010) Trace elements in organic-and iron-rich surficial fluids of the boreal zone: assessing colloidal forms via dialysis and ultrafiltration. Geochim Cosmochim Acta 74(2):449–468

Vindedahl AM, Strehlau JH, Arnold WA, Penn RL (2016) Organic matter and iron oxide nanoparticles: aggregation, interactions, and reactivity. Environ Sci Nano 3(3):494–505

von Wachenfeldt E, Tranvik LJ (2008) Sedimentation in boreal lakes—the role of flocculation of allochthonous dissolved organic matter in the water column. Ecosystems 11(5):803–814

Webb S (2005) SIXpack: a graphical user interface for XAS analysis using IFEFFIT. Phys Scr 2005(T115):1011

Weishaar JL, Aiken GR, Bergamaschi BA, Fram MS, Fujii R, Mopper K (2003) Evaluation of specific ultraviolet absorbance as an indicator of the chemical composition and reactivity of dissolved organic carbon. Environ Sci Technol 37(20):4702–4708

Weyhenmeyer GA, Prairie YT, Tranvik LJ (2014) Browning of boreal freshwaters coupled to carbon-iron interactions along the aquatic continuum. PLoS ONE 9(2):e88104. https://doi.org/10.1371/journal.pone.0088104

Whitty SD, Waggoner DC, Cory RM, Kaplan LA, Hatcher PG (2021) Direct noninvasive 1H NMR analysis of stream water DOM: Insights into the effects of lyophilization compared with whole water. Magn Reson Chem 59(5):540–553

Wilkinson KJ, Joz-Roland A, Buffle J (1997) Different roles of pedogenic fulvic acids and aquagenic biopolymers on colloid aggregation and stability in freshwaters. Limnol Oceanogr 42(8):1714–1724

Wilson M (1981) Applications of nuclear magnetic resonance spectroscopy to the study of the structure of soil organic matter. J Soil Sci 32(2):167–186

Xiao Y, Riise G (2021) Coupling between increased lake color and iron in boreal lakes. Sci Total Environ 767:145104

Xie H, Zafiriou OC, Cai W-J, Zepp RG, Wang Y (2004) Photooxidation and its effects on the carboxyl content of dissolved organic matter in two coastal rivers in the southeastern United States. Environ Sci Technol 38(15):4113–4119